PAPER

Magnetite nanoparticle anchored graphene cathode enhances microbial electrosynthesis of polyhydroxybutyrate by *Rhodopseudomonas* palustris TIE-1

To cite this article: Karthikeyan Rengasamy et al 2020 Nanotechnology 32 035103

View the article online for updates and enhancements.



IOP ebooks™

Bringing together innovative digital publishing with leading authors from the global scientific community.

Start exploring the collection-download the first chapter of every title for free.

IOP Publishing Nanotechnology

Nanotechnology 32 (2021) 035103 (14pp)

https://doi.org/10.1088/1361-6528/abbe58

Magnetite nanoparticle anchored graphene cathode enhances microbial electrosynthesis of polyhydroxybutyrate by *Rhodopseudomonas palustris* TIE-1

Karthikeyan Rengasamy¹, Tahina Ranaivoarisoa¹, Wei Bai^{1,2} and Arpita Bose¹

E-mail: abose@wustl.edu

Received 29 August 2020, revised 1 October 2020 Accepted for publication 5 October 2020 Published 22 October 2020



Abstract

Microbial electrosynthesis (MES) is an emerging technology that can convert carbon dioxide (CO₂) into value-added organic carbon compounds using electrons supplied from a cathode. However, MES is affected by low product formation due to limited extracellular electron uptake by microbes. Herein, a novel cathode was developed from chemically synthesized magnetite nanoparticles and reduced graphene oxide nanocomposite (rGO-MNPs). This nanocomposite was electrochemically deposited on carbon felt (CF/rGO-MNPs), and the modified material was used as a cathode for MES production. The bioplastic, polyhydroxybutyrate (PHB) produced by Rhodopseudomonas palustris TIE-1 (TIE-1), was measured from reactors with modified and unmodified cathodes. Results demonstrate that the magnetite nanoparticle anchored graphene cathode (CF/rGO-MNPs) exhibited higher PHB production (91.31 \pm 0.9 mg l⁻¹). This is \sim 4.2 times higher than unmodified carbon felt (CF), and 20 times higher than previously reported using graphite. This modified cathode enhanced electron uptake to $-11.7 \pm 0.1 \,\mu\mathrm{A\,cm}^{-2}$, ~ 5 times higher than CF cathode ($-2.3 \pm 0.08 \,\mu\mathrm{A\,cm}^{-2}$). The faradaic efficiency of the modified cathode was ~2 times higher than the unmodified cathode. Electrochemical analysis and scanning electron microscopy suggest that rGO-MNPs facilitated electron uptake and improved PHB production by TIE-1. Overall, the nanocomposite (rGO-MNPs) cathode modification enhances MES efficiency.

Keywords: magnetite nanoparticles, microbial electrosynthesis, *rhodopseudomonas palustris* TIE-1, polyhydroxybutyrate(PHB)

1

(Some figures may appear in colour only in the online journal)

1. Introduction

Growing energy needs and increasing CO₂ emissions have led to severe environmental problems such as a rise in global temperatures [1]. In order to counter CO₂ emissions, research geared toward the utilization of CO₂ (as a feedstock) via chemical, electrochemical, and biological technologies is

essential [2]. Current technologies require high energy input, large land area, or expensive catalysts [3]. Therefore, novel technologies are needed for CO₂ conversion/fixation. Microbial electrosynthesis (MES) is a promising new technology that can convert CO₂ into organic carbon compounds using autotrophic microbes that are capable of performing electron uptake and CO₂ conversion/fixation. Here, these

¹ Department of Biology, Washington University in Saint Louis, St. Louis, MO, 63130, United States of America

² Department of Energy, Environmental and Chemical Engineering, Washington University in St. Louis, St. Louis, MO, United States of America

microbes serve as biocatalysts in a bioelectrochemical systems [4–7]. Electrosynthesis by autotrophic microbes requires mild electrical power input to trigger the thermodynamically non-spontaneous reduction of CO₂ into organic carbon compounds [8]. In principle, autotrophic bacteria residing at the cathode (electrode) in MES utilize CO₂ as the sole carbon source to produce value added organic compounds such as acetate [9, 10], butyrate [11, 12], other volatile fatty acids (VFAs) [13], and polyhydroxy butyrate (PHB) [14, 15].

Several microbes can take up electrons from cathodes at different poised cathode potentials (PCP), and some studies show that they can perform MES. For example, the model metal reducing bacterium Shewanella oneidensis MR-1 can accept electrons from plain indium tin oxide at PCP of −0.303 V versus standard hydrogen electrode (SHE; hereafter all the potentials are relative to SHE unless otherwise noted) using the Mtr multiheme cytochrome c electron conduit [16]. Also, iron oxidizing bacteria such as Mariprofundus ferrooxydans [17] at PCP of -0.076 V and Acidithiobacillus ferroxidans [18] at PCP of +0.244 V were cultivated by electron uptake from a cathode. Sporomusa ovata and Clostridium spp. have been shown to produce acetate from CO₂ by accepting electrons at PCP of $-0.400\,\mathrm{V}$ via MES. For more examples of MES by other microbes, please read these recent reviews [5, 7, 8, 19].

Our research shows that the phototrophic iron oxidizing bacterium, Rhodopseudomonas palustris TIE-1 (TIE-1) can take up electrons directly from a poised electrode at PCP of +0.100 V while fixing CO₂ [20–22]. In these studies, the poised cathode is the only electron source and CO₂ is the sole carbon source for TIE-1. TIE-1 is an attractive model organism for bioproduction due to its metabolic versatility [23]. When grown photoautotrophically, TIE-1 can use multiple electron sources including hydrogen and soluble iron, Fe(II) [23], in addition to poised electrodes [20–22]. When TIE-1 uses Fe(II) as an electron donor for photoautotrophy, it produces goethite and magnetite [23]. Recent work from our group shows that the PioAB complex, which is related to the MtrCAB system of Shewanella sps., likely forms an electron conduit responsible for electron uptake from both Fe(II) and poised electrodes. PioB is an outer membrane porin associated with the decaheme cytochrome c protein, PioA [24]. There are several differences between the Mtr system of Shewanella and the Pio system of TIE-1. These include the lack of an extracellular multiheme cytochrome c protein (MtrC in Shewanella) in the Pio system and a large posttranslationally processed N-terminus in the PioA protein that is absent in the MtrA protein [24]. These differences might affect the manner in which these two microbes interact with iron oxides minerals.

We have also shown that TIE-1 can produce the bioplastic polyhydroxybutyrate (PHB) linked to electron uptake at a PCP of +0.100 V using CO₂ as the sole carbon source, thus demonstrating MES [15]. PHB is an attractive bioplastic naturally synthesized by many microorganisms [25–27]. It serves as a carbon and energy reserve in cells when microbes are grown under environmentally stressful conditions [28, 29]. PHB can be an alternative to non-biodegradable

plastics produced from petroleum [30, 31]. However, the major limitation for commercialization of PHB as a bioplastic is the associated high production cost [29, 32–34]. By using the low-cost feedstock CO₂ and abundant renewable resources such as sunlight and electricity, MES can lower PHB production cost [35–37]. However, in MES applications low electron uptake by microbes including TIE-1 leads to lower product formation [7, 19, 38–40]. Increasing electron-uptake is expected to improve the titer of products such as PHB during MES [41, 42].

Modification of the cathode surface to improve MES has been explored in a number of studies. Electrode (both cathode and anode) modifications include using nanoparticles, carbon nanomaterials, and conducting polymer composites [39, 42–50]. Studies have shown that modified cathode surfaces improve VFAs production via MES [39, 42, 44, 49]. Gold nanoparticle coated carbon cloth improves acetate production up to 6 times compared to unmodified carbon cloth $(30 \pm 7 - 181 \pm 44 \text{ mM m}^{-2} \text{ d}^{-1})$ [49]. Carbon nanotube coated electrodes can also improve acetate production via MES [51]. We have previously shown that using a graphite electrode coated with an insoluble iron oxide redox mediator, Prussian Blue, is an inexpensive way to increase electron uptake by TIE-1 by \sim 3.8 times. There was an enhanced cellular attachment of TIE-1 on the Prussian Blue-modified graphite electrode as well [22]. However, natural (semi)conductive iron minerals, such as magnetite produced by TIE-1 during photoautotrophic growth using Fe(II) [23] have not been tested previously for cathode modifications in PHB production via MES by TIE-1.

Due to their biocompatibility, conductivity, low toxicity, and large specific surface area, natural (semi)conductive iron (III) oxides such as magnetite have been used to increase extracellular electron transfer (EFT) [52–54]. Furthermore, it is non-toxic to microorganisms and can be artificially synthesized using a simple chemical precipitation method [55, 56]. Magnetite is desirable as iron oxide in EFT applications because of its unique magnetic and electrical properties based on the electron transfer between Fe(II) and Fe(III) in its octahedral sites [57]. In a relevant study, a Geobacter sulfurreducens mutant lacking the multiheme c-type cytochrome, OmcS, regained the ability to reduce Fe(III) to Fe(II) when magnetite was added only when the pilA gene, encoding the pilin protein, was present. This suggests that magnetite can compensate for the lack of OmcS in G. sulfurreducens as long as the cells contain the *pilA* gene [58]. To effectively use magnetite for MES applications it needs to be anchored to a supportive surface such as conductive carbon materials. Graphene has been recognized as a promising nanomaterial in electrochemical sensors because of its large surface area and exceptional electrical conductivity [50, 59-62]. We surmised that the integration of magnetite and graphene nanomaterials would improve the performance of the cathode in MES by

The present study focuses on improving PHB production from CO₂ via MES by TIE-1 using chemically synthesized magnetite nanoparticles (MNPs) and reduced graphene oxide (rGO). The obtained rGO-MNPs was attached to carbon felt

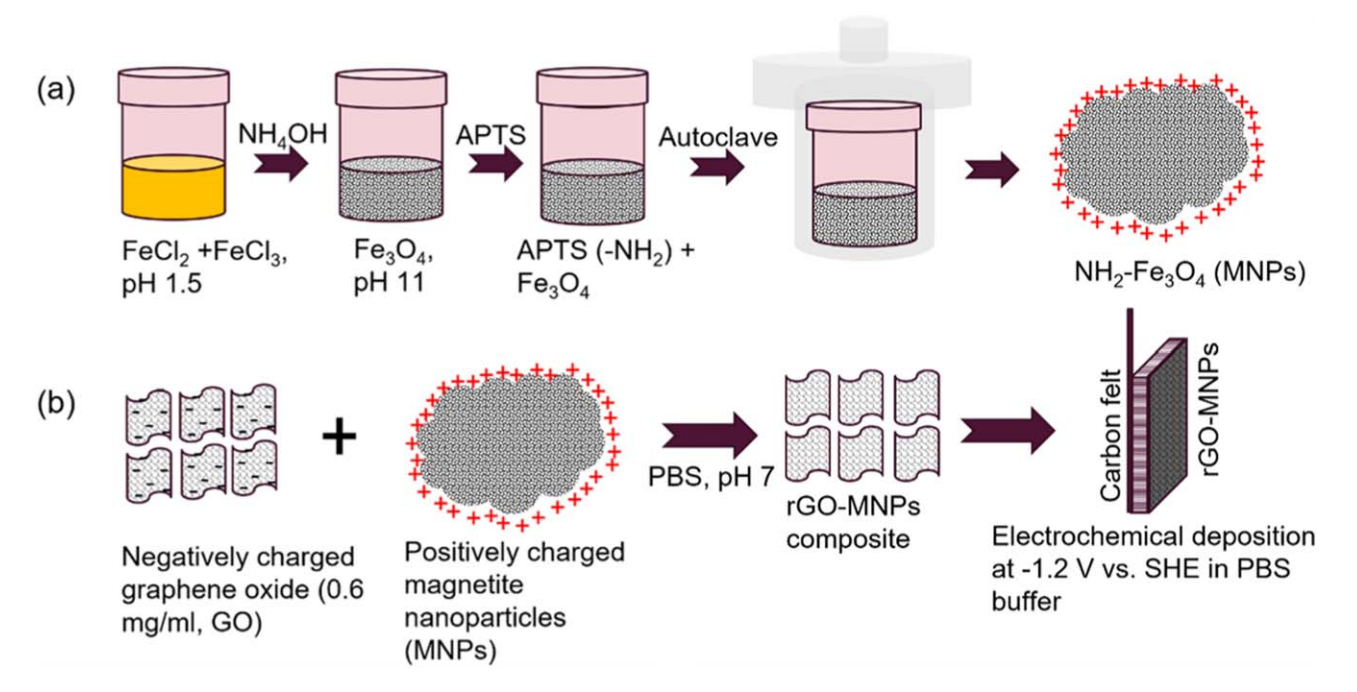


Figure 1. Schematic steps of nanocomposite synthesis and modified electrode fabrication. (a) Amine functionalized magnetite nanoparticle (MNPs) synthesis, and (b) Reduced graphene oxide-magnetite nanoparticle (rGO-MNPs) coating on carbon felt electrode fabrication. SHE: standard hydrogen electrode. APTS- 3-aminopropyltrimethoxysilane; PBS-phosphate buffer saline, Amine—NH₂; GO—Graphene oxide.

(CF) to create a new material, CF/rGO-MNPs. This modified electrode was used to assess electron uptake and PHB production in MES by TIE-1 in lab-scale reactors. The modified electrode, CF/rGO-MNPs, shows $\sim\!\!5$ times higher electron uptake and $\sim\!\!4.2$ times higher PHB production (91.31 \pm 0.9 mg l $^{-1}$) compared to the unmodified CF electrode. This improvement is $\sim\!\!20$ times higher than what we previously observed using unmodified graphite electrodes [63]. These lab-scale studies support the idea that electrode modifications using magnetite and graphene can be used to improve PHB production via MES in larger-scale platforms.

2. Experimental methods

2.1. Materials

Carbon felt substrate (AvCarb soft carbon felt) was purchased from Fuel cell earth, MA, USA. Water dispersed graphene oxide (4 mg ml⁻¹, Graphenea), Ferrous chloride tetrahydrate (FeCl₂. 4H₂O, Sigma-Aldrich), Ferric chloride hexachloride (FeCl₃.6H₂O, Alfa Aesar), Ammonia solution (NH₄OH, 28%, Alfa Aesar), 3-aminopropyltrimethoxysilane (APTS, Alfa Aesar) were purchased for nanocomposites synthesis.

2.2. Synthesis of the amine functionalized magnetite nanoparticles

Magnetite nanoparticles (MNPs or Fe_3O_4 NPs) were prepared via chemical co-precipitation method by mixing a 1:2 mol ratio mixture of ferrous (Fe^{2+}) and ferric (Fe^{3+}) salts (figure 1(a)). In a typical synthesis procedure, 1.5 g of $FeCl_2.4H_2O$ and 3.0 g of $FeCl_3$ were mixed in 100 ml of

water and vigorously stirred for 30 min at 60 °C under N₂ gas flow. Under this condition, 5 ml of NH₄OH was added to the solution via a syringe pump (Legato 110, KD Scientific, Inc.) at a rate of 0.5 ml min⁻¹ to precipitate MNPs. Next, the MNPs were collected from the solution and washed at least three times with Milli-Q water by the centrifugation-dispersion method at 5000 rpm for 15 min. Then the purified MNPs were dispersed in 15 ml of Milli-Q water and 1% 3-aminopropyltrimethoxysilane was added to functionalize positive charge (-NH₂ group) on MNPs [64]. This reaction mixture was then transferred into a Teflon-lined stainless pressure vessel and autoclaved at 90 °C for 3 h. Finally, a black precipitate consisting of the amine-functionalized magnetite nanoparticles (MNPs- NH₂) was purified with ethanol by the centrifugation-dispersion method and dried at 30 °C for 12 h.

2.3. Electrostatic assembly of rGO-MNPs composite and electrode fabrication

Amine functionalized MNPs were anchored on graphene oxide (GO) by the electrostatic assembly to avoid aggregation of magnetic particles (figure 1(b)). Wherein, 75 mg of amine-functionalized MNPs were added into 25 ml of GO solution (0.6 mg ml^{-1}) under mild magnetic stirring and the mixture was continuously stirred at room temperature for 12 h to form GO-MNPs composite mixture (5:1 ratio of MNPs and GO). This composite was used to fabricate a modified carbon felt electrode (cathode) for MES experiments. Typically, a piece of carbon felt $(1 \times 1 \text{ cm}^2)$, AvCarb soft carbon felt, Fuel cell earth) was electrically connected with titanium metal wire [65]. This carbon felt electrode was then immersed in the composites of GO-MNPs for 15 min and dried for 1 h at room

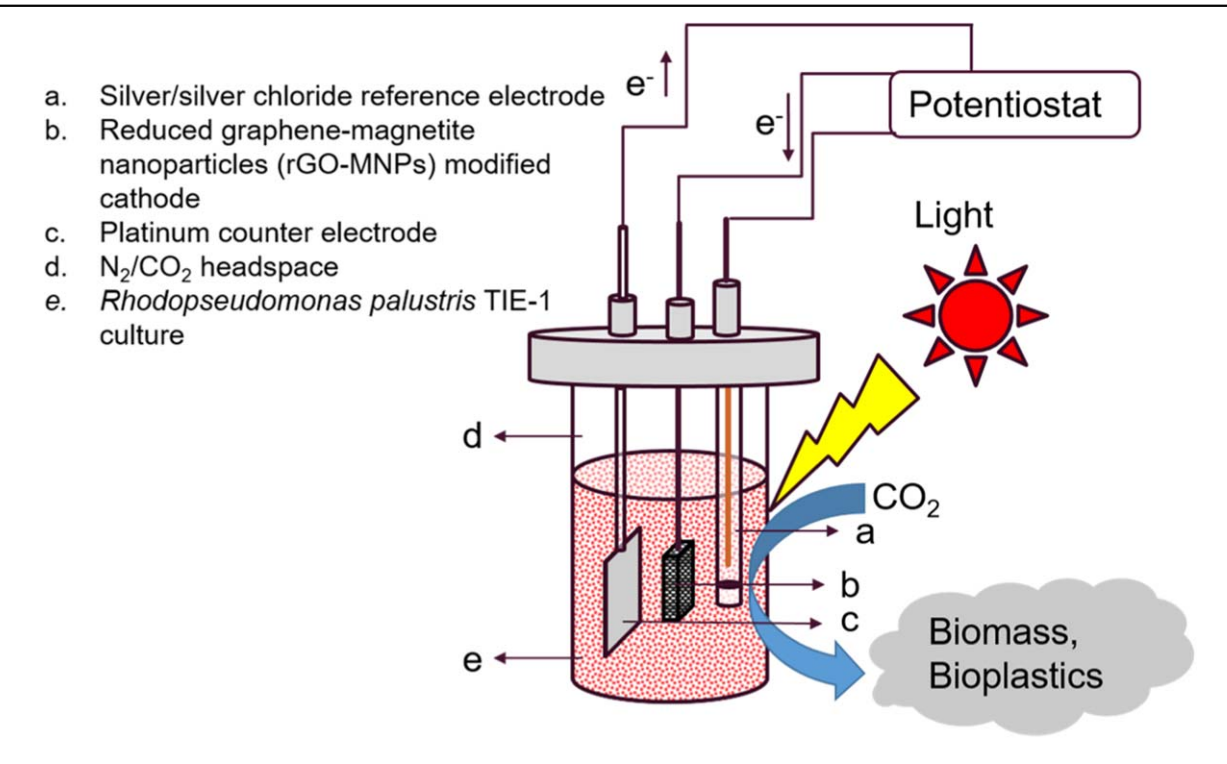


Figure 2. Schematic set up of the microbial electrosynthesis reactor for bioplastics production by *Rhodopseudomonas palustris* TIE-1. N₂—nitrogen; CO₂—carbon dioxide; e⁻—electron.

temperature (25 °C). This immersion and dry coating procedure were repeated twice in order to obtain the complete coating of the nanocomposites [46]. The coated carbon felt electrode was electrochemically reduced at the potential of $-1.212\,\mathrm{V}$ for 15 min and cycled (\sim 10 cycles) between $-1.212\,\mathrm{and}\,1.088\,\mathrm{V}$ in PBS buffer at a scan rate of $10\,\mathrm{mV}\,\mathrm{s}^{-1}$ using an electrochemical potentiostat (Gamry Multichannel potentiostat, USA). During this electrochemical reduction, the nanocomposite (rGO-MNPs) is successfully deposited on the carbon felt electrode. This modified carbon felt electrode was further characterized by both electrochemical and surface characterization prior to its use in MES experiments (figure 2).

2.4. SEM, XRD, Raman and FTIR characterizations

The morphology/size of the nanocomposites and its modification on carbon felt electrodes (before and after MES experiments) were analyzed by scanning electron microscopy (SEM, Thermofisher Quattro S ESEM) equipped with energy dispersive x-ray system (Oxford AzTec energy dispersive x-ray spectrometer). In order to image the microbial cells attached/enriched on the cathodes, a piece of the cathode was fixed with 5% glutaraldehyde for 15 min. Then the sample was gently rinsed with PBS solution, followed by serial dehydration of the sample with 50%, 60%, 70%, 80%, 90%, 95% and 100% ethanol [66]. At the end, the cathode samples were sputter-coated with 10 nm gold using a High Vacuum Sputter Coating system (Leica ACE 600) for SEM analysis. Powder x-ray diffraction (XRD, Bruker d8 Advance x-ray diffractometer) was used to determine the crystal structure of the magnetite sample. The Raman spectra were measured using a Renishaw inVia Raman system, 532 nm laser line for excitation and the wavenumber calibration was performed before the measurements. The Fourier-transform infrared (FTIR) spectra of the samples were recorded using an FTIR spectrometer (Thermo Scientific Nicolet 470).

2.5. MES experimental set up for polyhydroxybutyrate (PHB) production

MES experiments were conducted in a three-electrode (Pt as a counter electrode, Ag/AgCl as reference electrode 0.288 V versus SHE, and unmodified or modified carbon felt as working electrode or cathode) configured seal type electrolytic reactor (C001 Seal Electrolytic Cell, Xi'an Yima Optoelectrical Technology Com., Ltd, China). For MES experiments, 10 ml of wild type TIE-1 cells grown photoautotrophically on hydrogen in freshwater medium with sodium bicarbonate (22 mM) [15, 22] were inoculated in 70 ml of the same medium without hydrogen. The starting optical density $(OD_{660 \text{ nm}})$ of each inoculated reactor was set to be \sim 0.06. Further, the headspace gas of each MES reactor was purged with N_2/CO_2 (80%:20% at 48 kPa pressure) mixture. The performance of modified and unmodified carbon felt cathodes was evaluated by measuring electron uptake by TIE-1 (chronoamperometry analysis using Gamry multichannel potentiostat) at PCP of +0.100 V for 180 h [20]. We performed two sets of experiments for PHB synthesis: (1) using unmodified carbon felt (CF) and (2) using rGO-MNPs modified carbon felt (CF/rGO-MNPs) cathodes. All the MES experimental reactors were replicated (n = 3) at 25 °C unless noted otherwise.

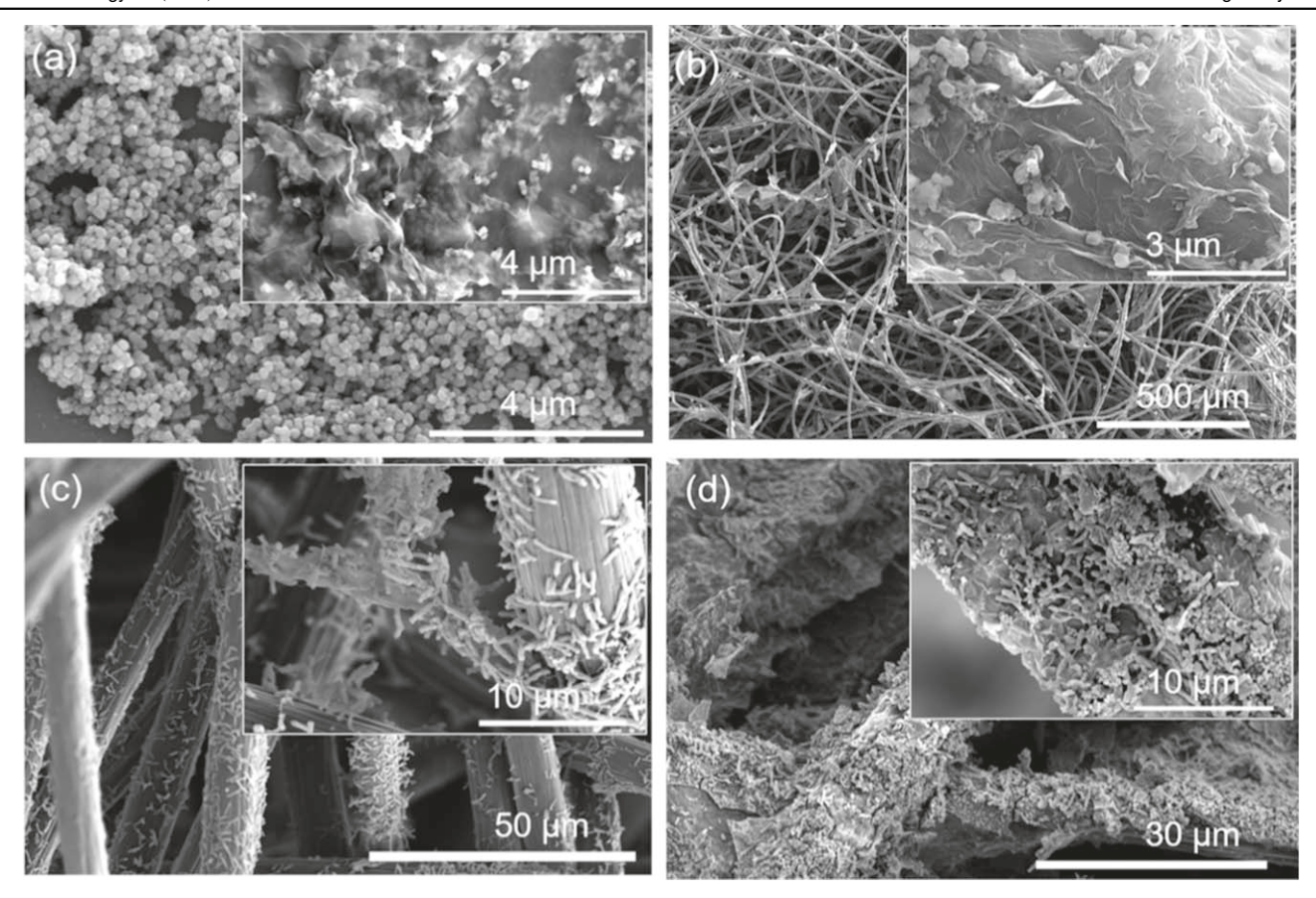


Figure 3. Scanning electron microscopy (SEM) images of magnetite nanoparticles (MNPs), reduced graphene oxide-magnetite nanoparticles (rGO-MNPs); and reduced graphene oxide with magnetite nanoparticles coated carbon felt (CF/rGO-MNPs) cathode prior to and after microbial electrosynthesis experiments. (a) Magnetite nanoparticles (MNPs), inset reduced graphene oxide-magnetite nanoparticles (rGO-MNPs); (b) reduced graphene oxide-magnetite nanoparticles electrodeposited on carbon felt (CF/rGO-MNPs), inset-magnified view of CF/rGO-MNPs. (c) Unmodified carbon felt (CF) electrode at the end of microbial electrosynthesis experiment, inset-magnified view; (d) reduced graphene oxide with magnetite nanoparticles modified electrode (CF/rGO-MNPs), inset- magnified view.

2.6. PHB analysis and faradaic efficiency

PHB measurement and faradaic efficiency from all MES reactors were performed at the end of the electron uptake experiment. A 10 ml bacterial sample was pelleted at 8000× g for 10 min and stored at -80 °C until PHB extraction and analysis were performed. 1 ml of water (LC-MS grade) and $600\,\mu l$ of methanol (HPLC grade) were added to arrest metabolic activity of TIE-1. 10 mg ml^{-1} of poly[(R)-3hydroxybutyric acid] (Sigma-Aldrich, USA) was used as a PHB standard. The extraction of PHB was followed by its conversion to crotonic acid. The concentration of crotonic acid was measured using an Agilent Technologies 6420 Triple Quad LC/MS as follows: using Hypercarb column, particle 5 μ m, 100 × 2.1 mm (Thermo Fisher Scientific, USA) as stationary phase; water with 0.1% (v/v) formic acid as phase A; acetonitrile and 1% (v/v) formic acid as phase B [3]. The injection volume was $5 \mu l$; the flow rate was set at $500 \,\mu\mathrm{l\,min}^{-1}$; the column temperature was set at 15 °C and the gas temperature was 300 °C. PHB was detected as crotonic acid with mass to charge ratio (m/z) = 87 which was normalized to bacterial cell number. PHB production efficiency was analyzed through their faradaic efficiency ($\eta\%$) [14, 67]. The faradaic efficiency was determined by the following formula

Faradaic efficiency
$$(\eta) = \frac{nzF}{\int idt}$$

' η ' faradaic efficiency, 'n' number of moles of the product, 'z' number of electrons transferred (18 e⁻ transferred from CO₂ to from crotonic acid), 'F' faradaic value (96 485 C mol⁻¹), 'i' is the current (A), and 'i' is the time (s).

3. Results and discussion

3.1. Morphology and electrostatic assembly of reduced graphene-magnetite nanoparticles (rGO-MNPs)

After the successful preparation of a nanocomposite, a number of characterization techniques were performed prior microbial electrosynthesis (MES). Figure 3 shows the SEM images of as-prepared magnetite nanoparticles (MNPs), reduced graphene-magnetite nanoparticles (rGO-MNPs) and their deposition on carbon felt (CF) electrode. As shown in figure 3(a), the MNPs were distributed uniformly with a size of 60–90 nm. These nanoparticles were observed as spherical

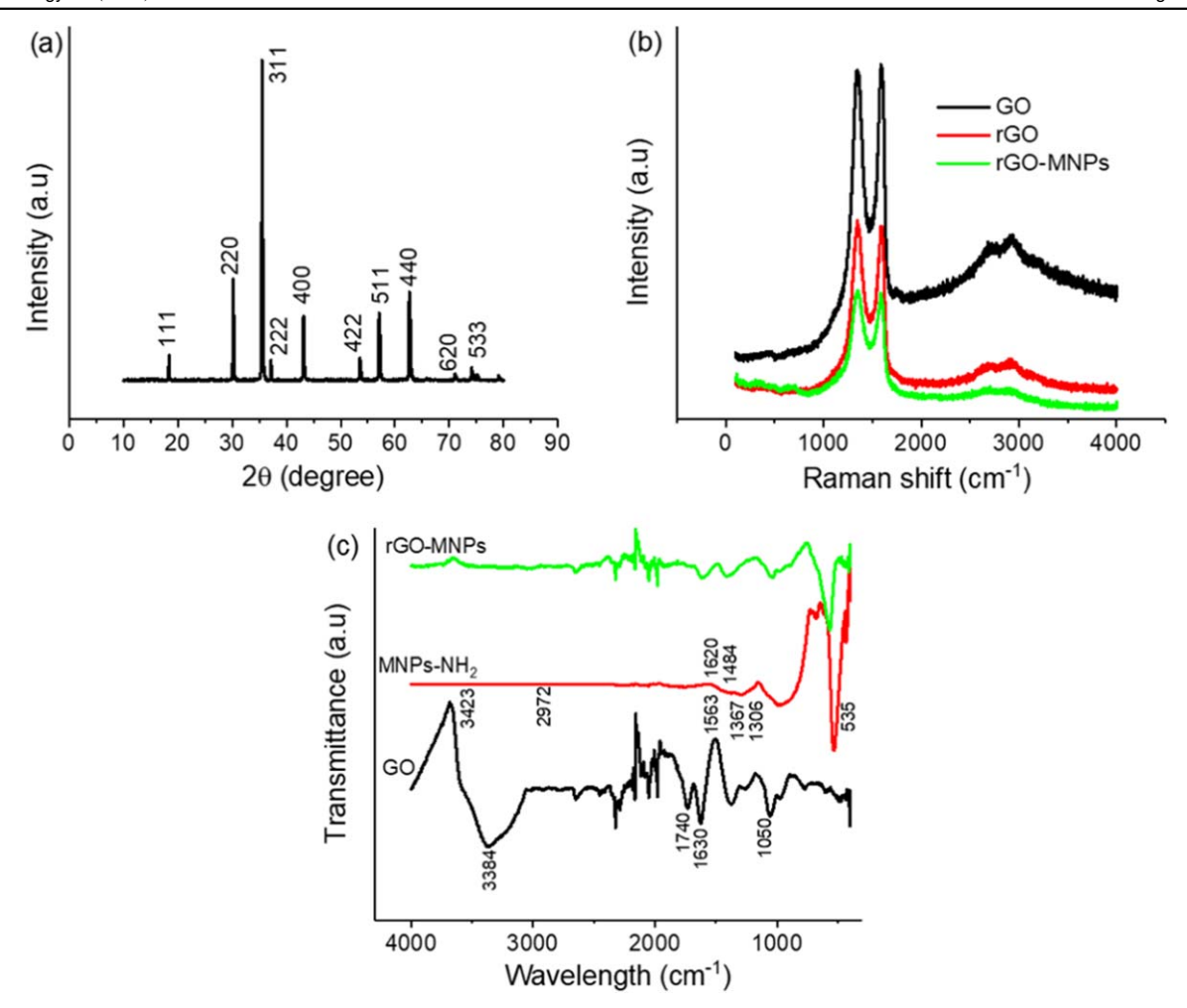


Figure 4. X-ray diffraction (XRD), Raman and Fourier transform Infrared (FTIR) spectroscopy of nanocomposite. (a) XRD pattern of magnetite nanoparticles; (b) Raman spectra of GO, rGO and rGO-MNPs; (c) FTIR spectra of GO, MNPs-NH₂ and rGO-MNPs. GO—graphene oxide; MNPs-NH₂—amine-functionalized magnetite nanoparticles; rGO-MNPs—nanocomposites of reduced graphene oxide with magnetite nanoparticles.

shaped particles that aggregated with each other due to the characteristic nature of magnetic dipole interactions [68]. The nanoparticles were uniformly anchored on the graphene layer indicating the formation of reduced graphene-magnetite (rGO-MNPs) nanocomposite by the electrostatic assembly as shown in insets of figure 3(a). This nanocomposite was successfully used to modify the carbon felt electrodes by an electrochemical reduction method as shown in figure 3(b). Further, prior to rGO-MNPs nanocomposite preparation XRD analysis was performed to confirm the crystallinity of the magnetite nanoparticles. Figure 4(a) shows the XRD pattern of the magnetite nanoparticles. Diffraction pattern appeared at 2θ of 18.35° , 30.14° , 35.50° , 37.12° , 43.15° , 53.48° , 57.03° , 62.65°, 71.01°, and 74.11° corresponding to the crystal plane of (111), (220), (311), (222), (400), (422), (511), (440), (620), and (533) the magnetite phase, respectively [69]. Characteristics of carbon atoms present in the GO, rGO and rGO-MNPs can be identified by Raman spectroscopy. As shown in figure 4(b), the characteristic carbon material D-band (disorder and defects, like disruption in the sp² bonding) and G-band (plane bond stretching motion of sp² hybridized carbon atoms) of the GO sample was present as 1349 cm⁻¹

and 1594 cm⁻¹ [70–72]. The intensity ratio of D and G band $(I_{\rm d}/I_{\rm g})$ was close to 0.89 in the case of GO sample. In contrast the intensity ratio $(I_{\rm d}/I_{\rm g})$ was increased in the case of rGO (1.02) and rGO-MNPs (1.03). This indicates that functional groups present in the graphene oxide dropped out when the GO was reduced to rGO [70]. The electrostatic assembly of MNPs and graphene oxide (GO) was analyzed by FTIR as shown in figure 4(c). The spectra in the presence of GO shows an absorption band at 3384 cm⁻¹, which was assigned to the -OH stretching vibration of alcoholic functional group, and the band at 1630 cm⁻¹ was attributed to the -COOH functional group [73]. In addition, the GO characteristic band at 1050 cm⁻¹, 1253 cm⁻¹, 1373 cm⁻¹ suggests the presence of C=O, C-O-C, C-OH groups [74]. The FTIR spectrum of amine-functionalized nanoparticles (MNPs-NH₂) shows the characteristic band at 535 cm⁻¹, which was attributed to the stretching vibration of Fe–O bonds in MNPs [75, 76]. Further, the two bands 3423 cm⁻¹ and 1620 cm⁻¹ can be assigned to the N-H stretching vibration and -NH₂ bending vibration, respectively. The stretching vibration of C-H at 2972 cm⁻¹, two bending vibrations of -CH₂ at 1484 cm⁻¹ and -CH₃ at 1367 cm⁻¹, and stretching vibration of C-N at 1306 cm⁻¹

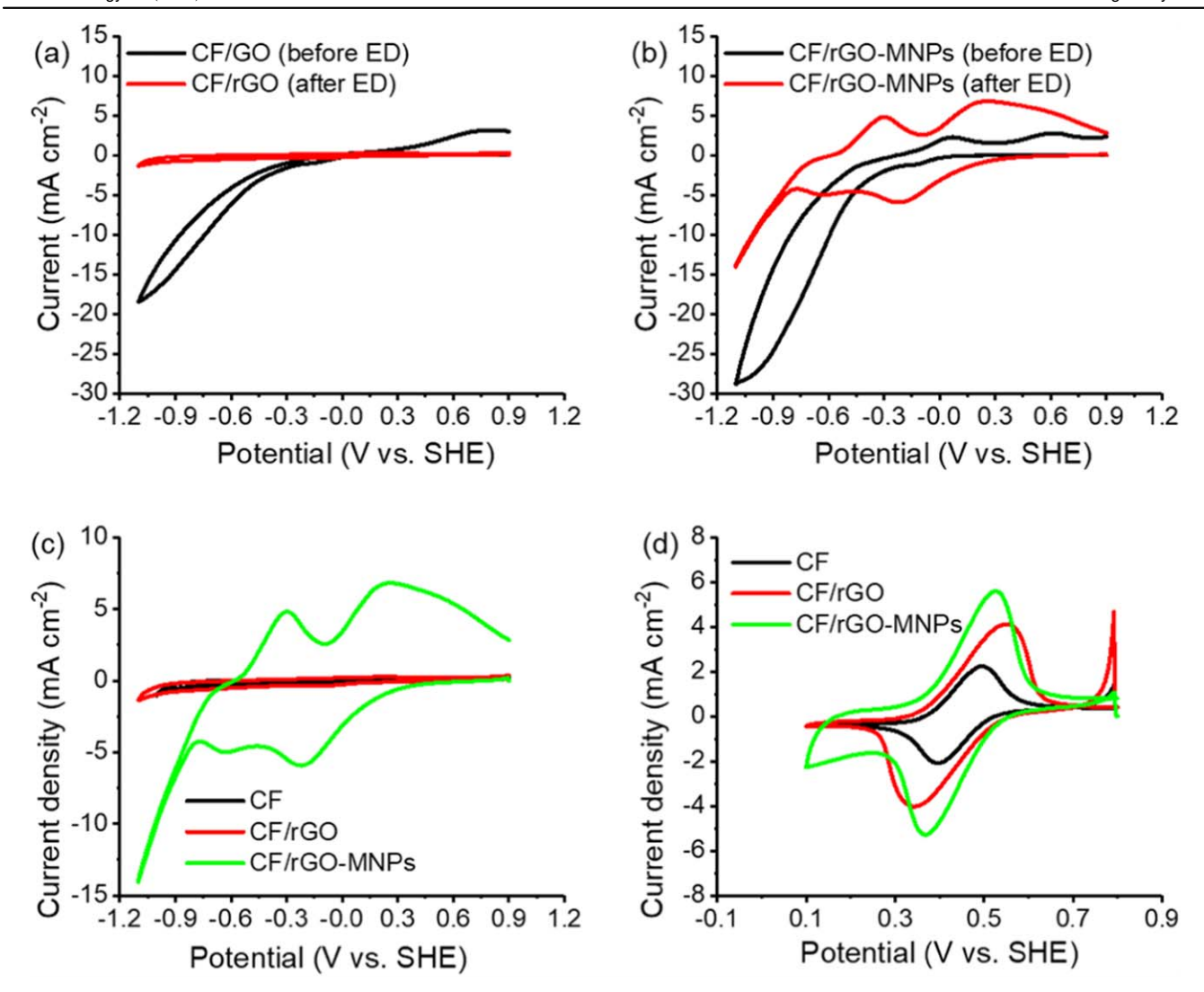


Figure 5. Representative cyclic voltammetry of modified and unmodified carbon felt (CF) electrode in phosphate-buffered saline (PBS) at a scan rate of 10 mV s^{-1} . (a) Before and after electrochemical deposition of the reduced graphene oxide (rGO) on CF electrode; (b) before and after electrochemical deposition of the reduced graphene oxide with magnetite nanoparticles (rGO-MNPs) on CF electrode; (c) comparison of modified (CF/rGO-MNPs), unmodified CF, and CF with reduced graphene oxide (CF/rGO) electrodes; (d) electrochemical characteristics of these three electrodes with 1 mM Fe(CN₆)^{3-/4-}. GO—graphene oxide; ED—electrochemical deposition; SHE—standard hydrogen electrode.

were observed in MNPs-NH₂ spectrum [77]. This result indicates that successful functionalization of the positive amine (-NH₂) group in MNPs was obtained using 3-aminopropyltrimethoxysilane. The FTIR spectrum of rGO-MNPs shows that the characteristic band for Fe–O shifted to 570 cm⁻¹, and peaks at 3384, 1050, 1253, 1630, and 1740 cm⁻¹ decreased when compared to the spectrum of GO. These results suggest that the oxygen-containing functional group in graphene oxide (GO) was reduced to graphene (rGO) with MNPs in the nanocomposite.

3.2. Electrochemical characterization of rGO and rGO-MNPs modified electrode

Electrodeposition of rGO and rGO-MNPs composite on carbon felt electrode was performed at a reductive potential of -1.2 V for 15 min (data not shown). To confirm the electrodeposition on CF electrodes, cyclic voltammetry (CV) was

performed as shown in figures 5(a), (b). This CV profile indicates that before electrodeposition, a wide cathodic reduction peak of about -0.7 V starting from -0.3 to -1.0 V was observed in the case of CF/rGO and CF/rGO-MNPs electrode. This wide cathodic peak disappeared after electrodeposition on both electrodes. The disappearance of the wide reduction peak was due to the large reduction of the surface oxygen group in rGO layer [78]. Also, after electrodeposition, the electrode CF/rGO-MNPs show a clear redox mid-point potential at +0.05 and -0.450 V. The peak current at this redox potential was significantly enhanced after electrodeposition of CF/rGO-MNPs electrode when compared to CF/rGO electrode. In addition, CVs of the unmodified CF, CF/rGO, and CF/rGO-MNPs electrodes clearly exhibit electrodeposition on the CF surface (figure 5(c)).

The CVs of unmodified CF, CF/rGO, and CF/rGO-MNPs electrodes were performed using a redox probe (1 mM

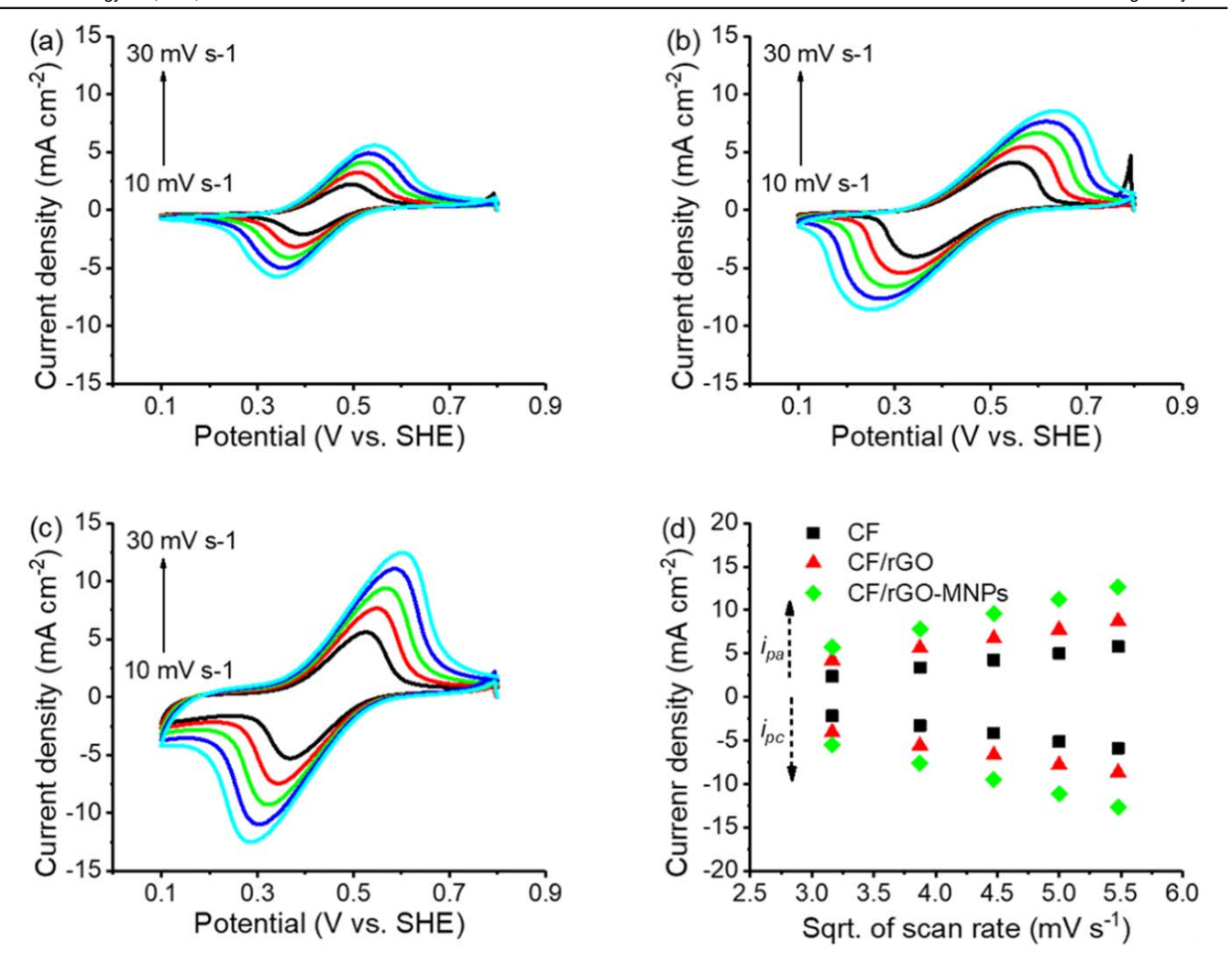


Figure 6. Cyclic voltammograms (CV) of the unmodified carbon felt (CF), CF with reduced graphene oxide (CF/rGO), and reduced graphene oxide with magnetite nanoparticles modified CF (CF/rGO-MNPs) electrodes in the presence of 1 mM [Fe(CN)₆]^{3-/4-} in 0.1 M NaCl solution at a scan rate of 10 mV s⁻¹. (a) unmodified CF electrode; (b) reduced graphene oxide (rGO) modified CF electrode (CF/rGO); (c) reduced graphene oxide with magnetite nanoparticles modified CF electrode (CF/rGO-MNPs); (d) square root of the scan rate versus cathodic and anodic peak current density (i_{pa} and i_{pc}) derived from CV analysis. SHE—standard hydrogen electrode; sqrt—square root.

 $Fe(CN_6)^{3-/4-})$ to calculate the electroactive surface area of the electrodeposited nanocomposites (figure 5(d)). The electroactive surface area of the CF/rGO-MNPs was calculated and compared with the unmodified CF electrode and the CF/rGO electrodes using the Randles–Sevcik equation from CVs analysis [59, 79]

$$i_{\rm pc} = 2.69 \times 10^5 \times n^{3/2} \times D^{1/2} \times v^{1/2} \times A \times C$$

where $i_{\rm pc}$ is the cathodic peak current (*A*); *n* is the number of electrons transferred; *D* is the diffusion coefficient $(7.6 \times 10^{-6} \ {\rm cm^2 \, s^{-1}})$; *v* is the scan rate (V s⁻¹); *A* is the electroactive area (cm²) and *C* is the concentration of the redox probe (mol cm⁻³). The cathodic peak current of the unmodified CF, CF/rGO and CF/rGO-MNPs were $-2.1075 \times 10^{-3} \, {\rm A}$, $-4.0091 \times 10^{-3} \, {\rm A}$, and $-5.3243 \times 10^{-3} \, {\rm A}$, respectively (figure 5(d)). Based on the Randles–Sevcik equation, the electroactive area of each electrode was calculated as follow, 0.326 cm² (CF) < 0.62 cm² (CF/rGO) < 0.824 cm² (CF/rGO-MNPs). The electroactive surface area of CF/rGO-MNPs was 2.53 times higher

than the unmodified CF electrode and 1.33 times higher than the CF/rGO electrode. These results indicate that the nanocomposite (rGO-MNPs) based electrode had a greatly enhanced electrochemical active area. Further, the scan rate dependent CVs of the carbon felt electrode (CF), CF/rGO, and CF/rGO-MNPs electrodes were analyzed in the presence of ferro/ferri redox probe (figures 6(a)-(c)). This study indicates that the anodic (i_{pa}) and cathodic peak current (i_{pc}) linearly increased by increasing the scan rate from 10 mV s to $30\,\mathrm{mV}\,\mathrm{s}^{-1}$ in all electrodes. The relationship between anodic and cathodic peak current of each electrode was plotted against the square root of scan rates (mV s⁻¹) in figure 6(d). The obtained peak currents (i_p) were linearly fitted to the scan rates (linear coefficient of 0.99). These results suggest that the electrochemical reaction at the electrodes are mainly diffusion-controlled. Higher peak current was observed in the case of CF/rGO-MNPs due to reduced diffusion, which leads to faster electron transfer [60, 80]. Also, the nanocomposite surface (CF/rGO-MNPs) provided better electroactivity than the rGO modified electrode. Therefore,

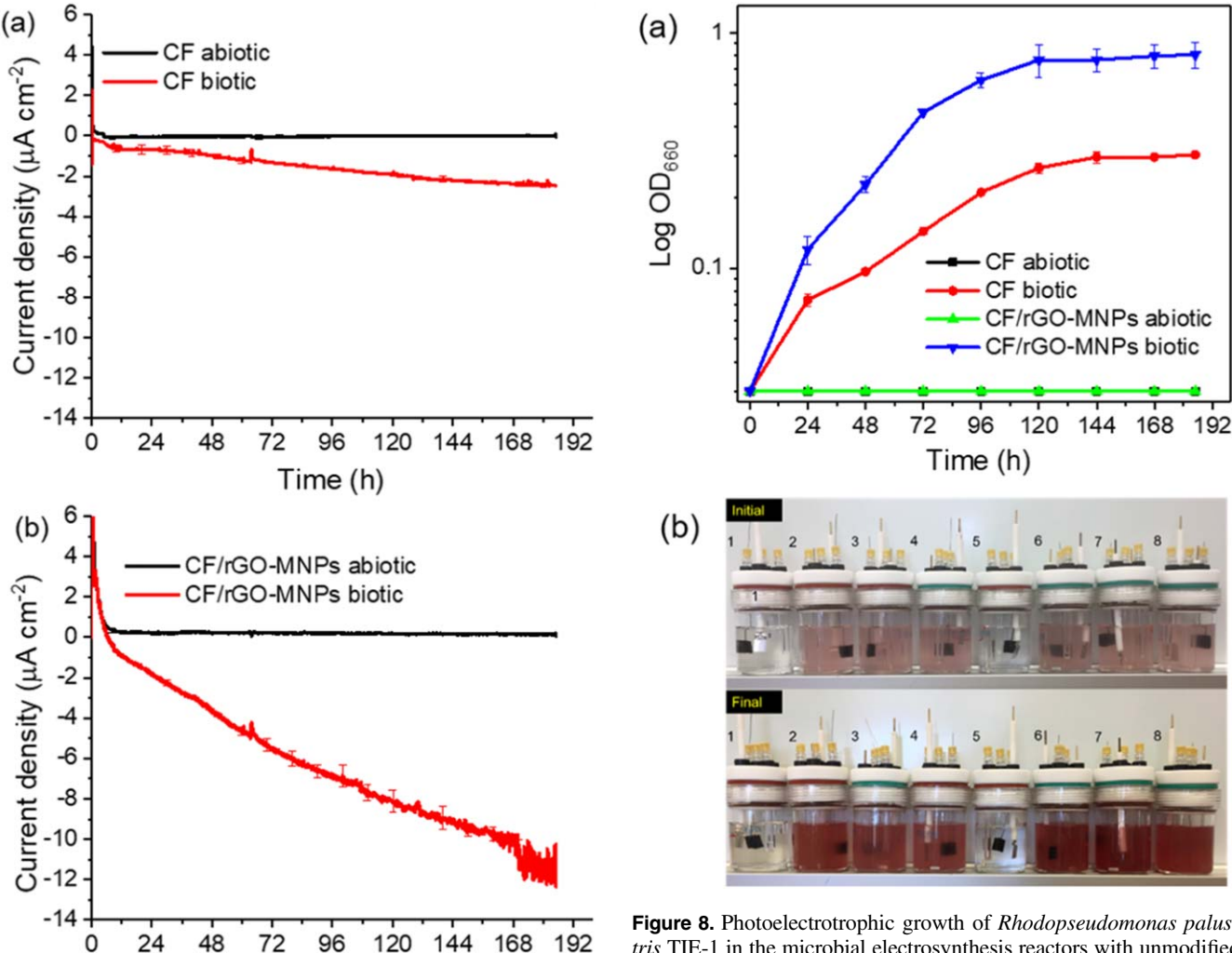


Figure 7. Electron uptake measurements of (a) unmodified carbon felt (CF) electrode, and (b) reduced graphene oxide with magnetite nanoparticles modified CF electrode (CF/rGO-MNPs) poised at +0.100 V versus standard hydrogen electrode in the presence and absence of *Rhodopseudomonas palustris* TIE-1. Biotic—TIE-1 inoculated reactor and abiotic—sterile control. Biotic data was collected from three biological replicates, and the error bar represents the standard deviation.

Time (h)

CF/rGO-MNPs electrode was used as cathode material to investigate the electron uptake and PHB synthesis in MES by TIE-1.

3.3. Electron uptake measurements and PHB synthesis

Based on electrochemical characterization, CF/rGO-MNPs and unmodified CF electrodes were chosen to investigate the performance in MES by TIE-1. The electron uptake measurements were conducted with nanocomposite modified electrodes (CF/rGO-MNPs) and unmodified CF electrodes using TIE-1 as a biocatalyst at PCP of +0.100 V as shown in figure 7. Herein, the cathodic current density increased on both modified and unmodified cathodes in the presence of TIE-1 in a biotic MES reactor. However, the cathodic current uptake of CF/rGO-MNPs (biotic) was higher than the

Figure 8. Photoelectrotrophic growth of *Rhodopseudomonas palustris* TIE-1 in the microbial electrosynthesis reactors with unmodified carbon felt (CF) electrode, and reduced graphene oxide with magnetite nanoparticles modified electrode (CF/rGO-MNPs). (a) Growth curves from different reactor set-ups; (b) Digital image of the reactors at the initial and final time. Reactor 1—unmodified CF electrode in an abiotic reactor; reactor 2, 3, 4—unmodified CF electrode in biotic reactors; reactor 5—reduced graphene oxide with magnetite nanoparticles modified electrode (CF/rGO-MNPs) in an abiotic reactor; reactor 6, 7, 8—reduced graphene oxide with magnetite nanoparticles modified electrode (CF/rGO-MNPs) in biotic reactors. Biotic data in figure (a) was collected from three biological replicates, and the error bar represents the standard deviation.

unmodified CF cathode (biotic). The maximum cathodic current density of $-11.7\pm0.1\,\mu\mathrm{A\,cm}^{-2}$ was for the CF/rGO-MNPs and $-2.3\pm0.08\,\mu\mathrm{A\,cm}^{-2}$ for the CF cathode. This cathodic current uptake $(-11.7\pm0.1\,\mu\mathrm{A\,cm}^{-2})$ in CF/rGO-MNPs was $\sim\!\!5$ times higher than the unmodified CF cathode. These results clearly reveal a significant difference in electron uptake from the nanocomposite modified electrode by TIE-1.

During the electron uptake measurements, growth measurements were also performed. Figure 8(a) shows the optical density (OD₆₆₀) of the MES reactors with modified and unmodified cathodes at different intervals. MES reactors reached a final OD₆₆₀ of 0.81 \pm 0.1 for CF/rGO-MNPs (biotic) and 0.30 \pm 0.01 for CF (biotic) cathodes when

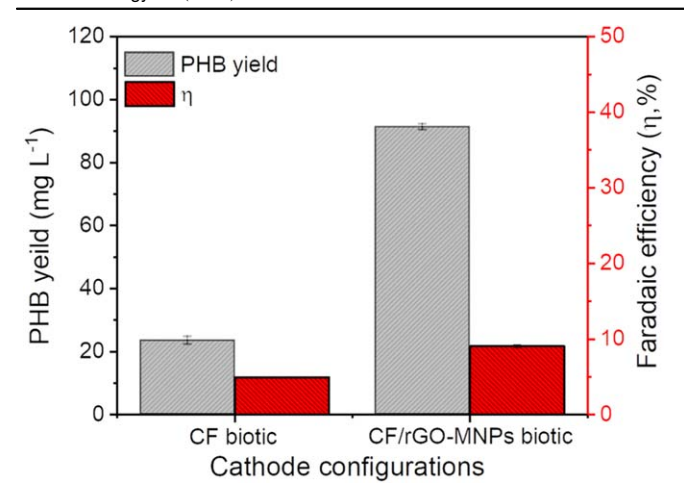


Figure 9. Polyhydroxybutyrate (PHB) yield and faradaic efficiency (η) of unmodified carbon felt (CF) electrode, and reduced graphene oxide with magnetite nanoparticles modified electrode (CF/rGO-MNPs) in the microbial electrosynthesis reactors. Data was collected from three biological replicates, and the error bar represents the standard deviation.

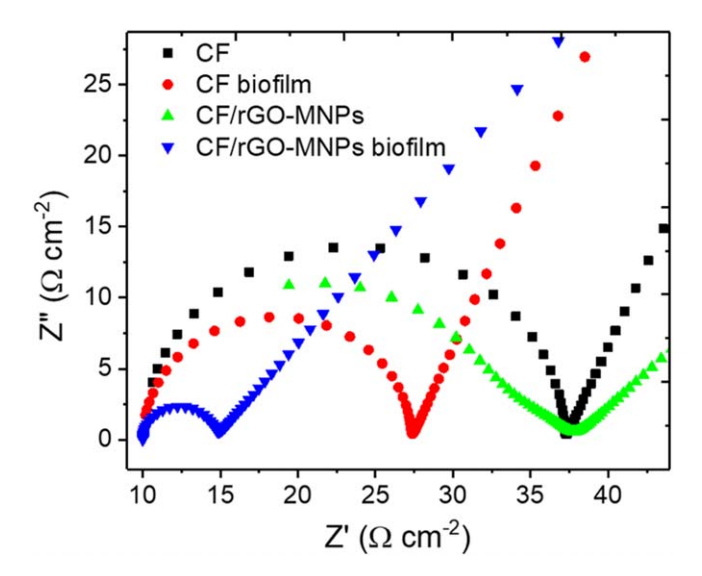


Figure 10. Electrochemical impedance spectra of reduced graphene oxide with magnetite nanoparticles modified electrode (CF/rGO-MNPs), and unmodified carbon felt electrode (CF) with or without an attached biofilm in the freshwater medium. CF-carbon felt; MNPs—magnetite nanoparticles; rGO—reduced graphene oxide.

compared to the abiotic reactors (0.02 \pm 0.001). These results suggest that biomass production was enhanced in CF/rGO-MNPs (biotic) reactors, as demonstrated in the digital images of MES reactors at the end of the electron uptake experiment (figure 8(b)). This microbial growth enhancement in the CF/ rGO-MNPs (biotic) reactor can be correlated to its higher electroactive surface [42, 61, 62].

The intracellular PHB accumulation and faradaic efficiency of both the CF cathode and the CF/rGO-MNPs cathode reactors were measured at the end of the electron uptake measurements as shown in figure 9. The modified CF/ rGO-MNPs (biotic) electrode had a PHB yield of $91.31 \pm 0.9 \,\mathrm{mg} \,\mathrm{l}^{-1}$ compared to $23.43 \pm 1.29 \,\mathrm{mg} \,\mathrm{l}^{-1}$ (pvalue < 0.005) from the CF biotic cathode. Also, the faradaic

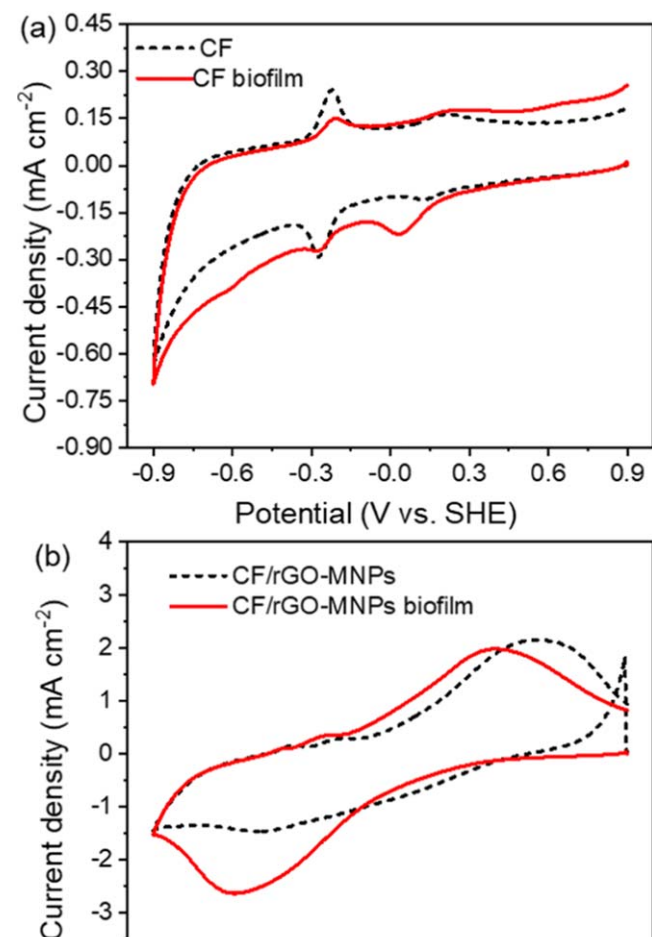


Figure 11. Cyclic voltammetry of biofilm enriched unmodified carbon felt electrode (CF) (a) and reduced graphene oxide with magnetite nanoparticles modified electrode (CF/rGO-MNPs) (b) in a freshwater medium at a scan rate of 5 mV s⁻¹. SHE—standard hydrogen electrode.

-0.3

-0.0

Potential (V vs. SHE)

0.3

0.6

0.9

-1

-2

-3

-0.9

-0.6

efficiency increased two times in the case of CF/rGO-MNPs (biotic) cathode (9.05% \pm 0.2%) compared to the CF biotic cathode (4.95% \pm 0.04%). The improved performance of the modified electrode may be due to lower charge transfer resistance and improved bioelectroactive sites of the biofilm in CF/rGO-MNPs cathode.

3.4. Bioelectroactivity of rGO-MNPs modified electrode

To investigate the bioelectroactivity of TIE-1, electrochemical impedance spectroscopy (EIS) and CV were performed on the biofilm-enriched cathode and biofilm-free cathode (abiotic) in a freshwater medium. EIS data from the cathodes were plotted as a Nyquist curve as shown figure 10. An equivalent circuit, $(R_s(C(R_{ct}W)))$ was used to derive the values of the circuit component. All the cathodes showed a typical semicircle at a high-frequency region and straight-line at a lower frequency region in EIS analysis. The value of charge transfers resistance (R_{ct}) between electrode and electrolyte can be calculated from the diameter of the semi-circle. Lower $R_{\rm ct}$ value (9 \pm 2 Ω cm⁻²) was obtained in the case of CF/rGO-MNPs with biofilm compared to the unmodified CF with biofilm (17 \pm 2 Ω cm⁻²) in the freshwater medium. The low R_{ct} value of the biofilm enriched CF/rGO-MNPs cathode could improve the EET, resulting in a higher electron uptake and PHB production via MES by TIE-1. Also, a higher capacitance (C) value was obtained from the biofilm enriched CF/rGO-MNPs cathode (52.06 \pm 3 mF cm⁻²) compared to the biofilm enriched CF cathode (5.31 \pm 0.7 mF cm⁻²). This higher capacitance of biofilm enriched CF/rGO-MNPs cathode correlated with a higher electroactive surface area of the nanocomposite. It has been reported that the high surface area of nanocomposite is favorable for microbial colonization, which leads to better biofilm formation, and faster substrate diffusion for bioelectrochemical reactions [50, 66, 81]. We observe that the electroactive moieties of biofilm enriched cathodes were analyzed in CV as shown in figure 11. A redox peak around 0.130 V was observed in the case of the CF biofilm, and 0.017 V from CF/rGO-MNPS biofilm, corresponding to the redox activity of TIE-1 [22]. Electroactive surface coverage of the biofilm on the cathodes can be obtained from the CV analysis (figure 11), and was calculated by using the surface coverage formula, $\Gamma = Q/nFA$, with charge involved on the active reduction peak area of the biofilm as Q, number of electrons involved in the reaction as n, Faraday constant (C mol^{-1}) as F, and area of the electrode (cm²) as A. The electroactive surface moieties of the biofilm on CF/rGO-MNPs cathode was $5.3472 \times 10^{-8} \,\mathrm{mol \, cm^{-2}}$ compared to $7.3160 \times 10^{-10} \text{ mol cm}^{-2}$ on the biofilm on CF cathode. This higher number of electroactive moieties at the rGO-MNPs composite can improve extracellular electron transfer leading to a more efficient synthesis of PHB [22, 82, 83]. The surface-attached biofilms on the unmodified (CF) and modified (CF/rGO-MNPs) cathodes were verified by using SEM as shown in figures 3(c), (d). The biofilm attached cells on both CF and CF/rGO-MNPs cathode appeared rod-shaped, similar to the previous reports of TIE-1 attached to cathodes [20, 22]. The biofilm attachment on CF cathode was less than the CF/rGO-MNPs cathode (figures 3(c), (d)). This likely leads to the higher value of electroactive surface coverage moieties obtained from electrochemical analyses. Therefore, rGO-MNPs modified CF is a superior cathodic material compared to the unmodified CF because it demonstrates an enhanced cellular attachment and higher electroactive surface moieties. Overall, this leads to improved MES performance and PHB production.

4. Conclusion

In this work, magnetite nanoparticle anchored graphene composite electrodeposited on carbon felt (CF/rGO-MNPs) was used as cathode material to increase electron uptake and polyhydroxybutyrate production by *Rhodopseudomonas palustris* TIE-1 via MES. The nanocomposite was prepared by a combination of amine-functionalized magnetite and graphene oxide. The nanocomposite modified cathode

improved extracellular electron uptake $(-11.7 \pm 0.1 \,\mu\text{A cm}^{-2}; \sim 4.2 \text{ higher than a CF cathode})$ and enhanced PHB production $(91.31 \pm 0.9 \,\mathrm{mg}\,\mathrm{l}^{-1})$; ~5 times higher than a CF cathode; 20 times higher than graphite [15] in TIE-1). There was an increased cellular attachment on the modified cathode suggesting a potential molecular interaction between magnetite and TIE-1. It has been observed that purified MtrC from Shewanella oneidensis MR-1 can make a specific bond with hematite, and this was suggested to be the basis for strong whole-cell interaction with hematite [84]. It is possible that components in the TIE-1 outer membrane (PioAB complex) might interact with magnetite leading to the improved attachment we observe here. This study sets the stage for future investigations into the interaction of TIE-1 with magnetite. Based on this study, we suggest that rGO-MNPs when electrodeposited on carbon felt can be a promising cathode material in MES. Future studies will focus on understanding the basis of the observed increase in extracellular electron uptake and the concomitant increase in bioplastic production.

Acknowledgments

The authors would like to acknowledge financial support from the US Department of Energy to A B (Grant number DESC0014613), the David and Lucile Packard Foundation to A B (Grant number 201563111), the Gordon and Betty Moore Foundation to A B, the US Department of Defense, Army Research Office to A B (Grant number W911NF-18-1-0037) and the National Science Foundation to A B (Grant number 2021822). Part of this work was performed under the auspices of the US Department of Energy by Lawrence Livermore National Laboratory under Contract DEAC5207NA27344 to A B. We would also like to thank Dr Rajesh Singh for indexing the XRD pattern and Eric Conners for the feedback on the manuscript, Washington University in St. Louis, USA.

ORCID iDs

Arpita Bose https://orcid.org/0000-0002-7526-0988

References

- [1] Jiang Y, Chu N, Qian D-K and Jianxiong Zeng R 2020 Microbial electrochemical stimulation of caproate production from ethanol and carbon dioxide *Bioresource Technol.* 295 122266
- [2] Mikkelsen M, Jørgensen M and Krebs F C 2010 The teraton challenge. A review of fixation and transformation of carbon dioxide *Energy Environ. Sci.* 3 43–81
- [3] Pearson R J, Eisaman M D, Turner J W G, Edwards P P, Jiang Z, Kuznetsov V L, Littau K A, Di Marco L and Taylor S R G 2012 Energy storage via carbon-neutral fuels made from CO₂, water, and renewable energy *Proc. IEEE* 100 440–60

- [4] Gadkari S, Shemfe M, Modestra J A, Mohan S V and Sadhukhan J 2019 Understanding the interdependence of operating parameters in microbial electrosynthesis: a numerical investigation *Phys. Chem. Chem. Phys.* 21 10761–72
- [5] Karthikeyan R, Singh R and Bose A 2019 Microbial electron uptake in microbial electrosynthesis: a mini-review *J. Ind. Microbiol. Biotechnol.* 46 1419–26
- [6] Mayr J C, Grosch J-H, Hartmann L, Rosa L F M, Spiess A C and Harnisch F 2019 Resting *Escherichia coli* as chassis for microbial electrosynthesis: production of chiral alcohols *ChemSusChem* 12 1631–4
- [7] Tremblay P L and Zhang T 2015 Electrifying microbes for the production of chemicals *Front. Microbiol.* **6** 201
- [8] Jiang Y and Jianxiong Zeng R 2018 Expanding the product spectrum of value added chemicals in microbial electrosynthesis through integrated process design—a review *Bioresource Technol.* 269 503–12
- [9] Gildemyn S, Verbeeck K, Slabbinck R, Andersen S J, Prévoteau A and Rabaey K 2015 Integrated production, extraction, and concentration of acetic acid from CO₂ through microbial electrosynthesis *Environ. Sci. Tech. Lett.* 2 325–8
- [10] Nevin K P, Woodard T L, Franks A E, Summers Z M and Lovley D R 2010 Microbial electrosynthesis: feeding microbes electricity to convert carbon dioxide and water to multicarbon extracellular organic compounds *mbio* 1 e00103–10
- [11] Batlle-Vilanova P, Ganigue R, Ramio-Pujol S, Baneras L, Jimenez G, Hidalgo M, Balaguer M D, Colprim J and Puig S 2017 Microbial electrosynthesis of butyrate from carbon dioxide: production and extraction *Bioelectrochemistry* 117 57-64
- [12] Ganigue R, Puig S, Batlle-Vilanova P, Balaguer M D and Colprim J 2015 Microbial electrosynthesis of butyrate from carbon dioxide *Chem. Commun.* 51 3235–8
- [13] Modestra J A, Navaneeth B and Mohan S V 2015 Bioelectrocatalytic reduction of CO₂: enrichment of homoacetogens and pH optimization towards enhancement of carboxylic acids biosynthesis J. CO₂ Utilization 10 78–87
- [14] Chen X, Cao Y, Li F, Tian Y and Song H 2018 Enzymeassisted microbial electrosynthesis of poly(3hydroxybutyrate) via CO₂ bioreduction by engineered Ralstonia eutropha ACS Catal. 8 4429–37
- [15] Ranaivoarisoa T O, Singh R, Rengasamy K, Guzman M S and Bose A 2019 Towards sustainable bioplastic production using the photoautotrophic bacterium *Rhodopseudomonas* palustris TIE-1 J. Ind. Microbiol. Biotechnol. 46 1–17
- [16] Rowe A R, Rajeev P, Jain A, Pirbadian S, Okamoto A, Gralnick J A, El-Naggar M Y and Nealson K H 2018 Tracking electron uptake from a cathode into *Shewanella* cells: implications for energy acquisition from solidsubstrate electron donors *mbio* 9 e02203–17
- [17] Summers Z M, Gralnick J A and Bond D R 2013 Cultivation of an obligate Fe(II)-oxidizing lithoautotrophic bacterium using electrodes mBio 4 e00420
- [18] Carbajosa S, Malki M, Caillard R, Lopez M F, Palomares F J, Martín-Gago J A, Rodríguez N, Amils R, Fernández V M and De Lacey A L 2010 Electrochemical growth of *Acidithiobacillus ferrooxidans* on a graphite electrode for obtaining a biocathode for direct electrocatalytic reduction of oxygen *Biosens. Bioelectron.* 26 877–80
- [19] Bian B, Bajracharya S, Xu J, Pant D and Saikaly P E 2020 Microbial electrosynthesis from CO₂: challenges, opportunities and perspectives in the context of circular bioeconomy *Bioresource Technol.* 302 122863

- [20] Bose A, Gardel E J, Vidoudez C, Parra E A and Girguis P R 2014 Electron uptake by iron-oxidizing phototrophic bacteria Nat. Commun. 5 3391
- [21] Guzman M S, Rengasamy K, Binkley M M, Jones C, Ranaivoarisoa T O, Singh R, Fike D A, Meacham J M and Bose A 2019 Phototrophic extracellular electron uptake is linked to carbon dioxide fixation in the bacterium Rhodopseudomonas palustris Nat. Commun. 10 1355
- [22] Rengasamy K, Ranaivoarisoa T, Singh R and Bose A 2018 An insoluble iron complex coated cathode enhances direct electron uptake by *Rhodopseudomonas palustris* TIE-1 *Bioelectrochemistry* 122 164–73
- [23] Jiao Y, Kappler A, Croal L R and Newman D K 2005 Isolation and characterization of a genetically tractable photoautotrophic Fe (II)-oxidizing bacterium, *Rhodopseudomonas palustris* strain TIE-1 *Appl. Environ. Microbiol.* 71 4487–96
- [24] Gupta D, Sutherland M C, Rengasamy K, Meacham J M, Kranz R G and Bose A 2019 Photoferrotrophs produce a PioAB electron conduit for extracellular electron uptake mBio 10 e02668
- [25] Jiang Y, Marang L, Kleerebezem R, Muyzer G and van Loosdrecht M C 2011 Polyhydroxybutyrate production from lactate using a mixed microbial culture *Biotechnol*. *Bioeng*. 108 2022–35
- [26] Kaewbai-Ngam A, Incharoensakdi A and Monshupanee T 2016 Increased accumulation of polyhydroxybutyrate in divergent cyanobacteria under nutrient-deprived photoautotrophy: an efficient conversion of solar energy and carbon dioxide to polyhydroxybutyrate by *Calothrix* scytonemicola TISTR 8095 Bioresource Technol. 212 342–7
- [27] Koutinas A A, Xu Y, Wang R and Webb C 2007 Polyhydroxybutyrate production from a novel feedstock derived from a wheat-based biorefinery *Enzyme Microb*. *Technol.* 40 1035–44
- [28] Luengo J M, García B, Sandoval A, Naharro G and Olivera E A R 2003 Bioplastics from microorganisms Curr. Opin. Microbiol. 6 251–60
- [29] Verlinden R A, Hill D J, Kenward M A, Williams C D and Radecka I 2007 Bacterial synthesis of biodegradable polyhydroxyalkanoates J. Appl. Microbiol. 102 1437–49
- [30] Jiang M, Chen J-N, He A-Y, Wu H, Kong X-P, Liu J-L, Yin C-Y, Chen W-F and Chen P 2014 Enhanced acetone/ butanol/ethanol production by *Clostridium beijerinckii* IB4 using pH control strategy *Process Biochem.* 49 1238–44
- [31] Wu H, Chen X P, Liu G P, Jiang M, Guo T, Jin W Q, Wei P and Zhu D W 2012 Acetone-butanol-ethanol (ABE) fermentation using *Clostridium acetobutylicum* XY16 and *in situ* recovery by PDMS/ceramic composite membrane *Bioproc. Biosyst. Eng.* 35 1057–65
- [32] Arrieta M P, Castro-López M D M, Rayón E, Barral-Losada L F, López-Vilariño J M, López J and González-Rodríguez M V 2014 Plasticized poly(lactic acid)-poly(hydroxybutyrate) (PLA-PHB) blends incorporated with catechin intended for active foodpackaging applications J. Agric. Food Chem. 62 10170–80
- [33] Getachew A and Woldesenbet F 2016 Production of biodegradable plastic by polyhydroxybutyrate (PHB) accumulating bacteria using low cost agricultural waste material BMC Res. Notes 9 509
- [34] Manikandan N A, Pakshirajan K and Pugazhenthi G 2020
 Preparation and characterization of environmentally safe and highly biodegradable microbial polyhydroxybutyrate (PHB) based graphene nanocomposites for potential food packaging applications *Int. J. Biol. Macromol.* **154** 866–77
- [35] Hou Y, Zhang R, Yu Z, Huang L, Liu Y and Zhou Z 2017 Accelerated azo dye degradation and concurrent hydrogen production in the single-chamber photocatalytic microbial electrolysis cell *Bioresource Technol.* **224** 63–8

- [36] Kong F, Ren H-Y, Pavlostathis S G, Nan J, Ren N-Q and Wang A 2020 Overview of value-added products bioelectrosynthesized from waste materials in microbial electrosynthesis systems *Renew. Sust. Energy Rev.* 125 109816
- [37] Prévoteau A, Carvajal-Arroyo J M, Ganigué R and Rabaey K 2020 Microbial electrosynthesis from CO₂: forever a promise? Curr. Opin. Biotechnol. 62 48–57
- [38] Aryal N, Ammam F, Patil S A and Pant D 2017 An overview of cathode materials for microbial electrosynthesis of chemicals from carbon dioxide *Green Chem.* 19 5748–60
- [39] Cui M, Nie H, Zhang T, Lovley D and Russell T P 2017 Threedimensional hierarchical metal oxide-carbon electrode materials for highly efficient microbial electrosynthesis Sustain. Energy Fuels 1 1171–6
- [40] Song T-S, Wang G, Wang H, Huang Q and Xie J 2019 Experimental evaluation of the influential factors of acetate production driven by a DC power system via CO₂ reduction through microbial electrosynthesis *Bioresource Bioproc*. 6 29
- [41] Chen L F, Tremblay P L, Mohanty S, Xu K and Zhang T 2016 Electrosynthesis of acetate from CO₂ by a highly structured biofilm assembled with reduced graphene oxidetetraethylene pentamine J. Mater. Chem. A 4 8395–401
- [42] Tahir K, Miran W, Jang J, Shahzad A, Moztahida M, Kim B and Lee D S 2020 A novel MXene-coated biocathode for enhanced microbial electrosynthesis performance *Chem. Eng. J.* 381 122687
- [43] Aryal N, Wan L L, Overgaard M H, Stoot A C, Chen Y M, Tremblay P L and Zhang T 2019 Increased carbon dioxide reduction to acetate in a microbial electrosynthesis reactor with a reduced graphene oxide-coated copper foam composite cathode *Bioelectrochemistry* 128 83–93
- [44] Jourdin L, Freguia S, Donose B C, Chen J, Wallace G G, Keller J and Flexer V 2014 A novel carbon nanotube modified scaffold as an efficient biocathode material for improved microbial electrosynthesis *J. Mater. Chem.* A 2 13093–102
- [45] Karthikeyan R, Ganesh V and Berchmans S 2012 Bioelectrocatalysis of Acetobacter aceti through direct electron transfer using a template deposited nickel anode Catal. Sci. Technol. 2 1234–41
- [46] Li Q, Fu Q, Kobayashi H, He Y, Li Z, Li J, Liao Q and Zhu X 2020 GO/PEDOT modified biocathodes promoting CO₂ reduction to CH₄ in microbial electrosynthesis Sustain. Energy Fuels 4 2987–97
- [47] Nie H R, Zhang T, Cui M M, Lu H Y, Lovley D R and Russell T P 2013 Improved cathode for high efficient microbial-catalyzed reduction in microbial electrosynthesis cells *Phys. Chem. Chem. Phys.* 15 14290–4
- [48] Ortiz-Martínez V M, Gajda I, Salar-García M J, Greenman J, Hernández-Fernández F J and Ieropoulos I 2016 Study of the effects of ionic liquid-modified cathodes and ceramic separators on MFC performance *Chem. Eng. J.* 291 317–24
- [49] Zhang T, Nie H R, Bain T S, Lu H Y, Cui M M, Snoeyenbos-West O L, Franks A E, Nevin K P, Russell T P and Lovley D R 2013 Improved cathode materials for microbial electrosynthesis *Energy Environ. Sci.* 6 217–24
- [50] Zhang Y, Liu L, Van der Bruggen B and Yang F 2017 Nanocarbon based composite electrodes and their application in microbial fuel cells *J. Mater. Chem.* A 5 12673–98
- [51] Flexer V and Jourdin L 2020 Purposely designed hierarchical porous electrodes for high rate microbial electrosynthesis of acetate from carbon dioxide Acc. Chem. Res. 53 311–21
- [52] Guo J et al 2017 Polypyrrole-interface-functionalized nanomagnetite epoxy nanocomposites as electromagnetic wave

- absorbers with enhanced flame retardancy *J. Mater. Chem.* C **5** 5334–44
- [53] Li Y *et al* 2018 3D magnetic graphene oxide-magnetite poly (vinyl alcohol) nanocomposite substrates for immobilizing enzyme *Polymer* **149** 13–22
- [54] Lower S K, Hochella M F and Beveridge T J 2001 Bacterial recognition of mineral surfaces: nanoscale interactions between *Shewanella* and α-FeOOH Science 292 1360–3
- [55] Park I H, Christy M, Kim P and Nahm K S 2014 Enhanced electrical contact of microbes using Fe₃O₄/CNT nanocomposite anode in mediator-less microbial fuel cell *Biosens. Bioelectron.* 58 75–80
- [56] Peng X, Yu H, Wang X, Zhou Q, Zhang S, Geng L, Sun J and Cai Z 2012 Enhanced performance and capacitance behavior of anode by rolling Fe₃O₄ into activated carbon in microbial fuel cells *Bioresource Technol.* 121 450–3
- [57] Zhang Z J, Chen X Y, Wang B N and Shi C W 2008 Hydrothermal synthesis and self-assembly of magnetite (Fe₃O₄) nanoparticles with the magnetic and electrochemical properties J. Cryst. Growth 310 5453-7
- [58] Liu F, Rotaru A E, Shrestha P M, Malvankar N S, Nevin K P and Lovley D R 2015 Magnetite compensates for the lack of a pilin-associated c-type cytochrome in extracellular electron exchange *Environ. Microbiol.* 17 648–55
- [59] He Q, Liu J, Liu X, Li G, Chen D, Deng P and Liang J 2018 Fabrication of amine-modified magnetite-electrochemically reduced graphene oxide nanocomposite modified glassy carbon electrode for sensitive dopamine determination *Nanomaterials* 8 194
- [60] Salamon J, Sathishkumar Y, Ramachandran K, Lee Y S, Yoo D J, Kim A R and Gnana Kumar G 2015 One-pot synthesis of magnetite nanorods/graphene composites and its catalytic activity toward electrochemical detection of dopamine *Biosens. Bioelectron.* 64 269–76
- [61] Wang H, Wang G, Ling Y, Qian F, Song Y, Lu X, Chen S, Tong Y and Li Y 2013 High power density microbial fuel cell with flexible 3D graphene-nickel foam as anode *Nanoscale* 5 10283–90
- [62] Yong Y C, Yu Y Y, Zhang X H and Song H 2014 Highly active bidirectional electron transfer by a self-assembled electroactive reduced-graphene-oxide-hybridized biofilm** Angew. Chem., Int. Ed. 53 4480-3
- [63] Ranaivoarisoa T O, Singh R, Rengasamy K, Guzman M S and Bose A 2019 Towards sustainable bioplastic production using the photoautotrophic bacterium *Rhodopseudomonas* palustris TIE-1 J. Ind. Microbiol. Biotechnol. 46 1401–17
- [64] Li K, Shen M, Zheng L, Zhao J, Quan Q, Shi X and Zhang G 2014 Magnetic resonance imaging of glioma with novel APTS-coated superparamagnetic iron oxide nanoparticles *Nanoscale Res. Lett.* 9 304
- [65] Milner E M, Scott K, Head I M, Curtis T and Yu E H 2017 Evaluation of porous carbon felt as an aerobic biocathode support in terms of hydrogen peroxide J. Power Sources 356 459–66
- [66] Karthikeyan R, Wang B, Xuan J, Wong J W C, Lee P K H and Leung M K H 2015 Interfacial electron transfer and bioelectrocatalysis of carbonized plant material as effective anode of microbial fuel cell *Electrochim. Acta* 157 314–23
- [67] Lv W, Zhang R, Gao P and Lei L 2014 Studies on the faradaic efficiency for electrochemical reduction of carbon dioxide to formate on tin electrode J. Power Sources 253 276–81
- [68] Mørup S, Hansen M F and Frandsen C 2010 Magnetic interactions between nanoparticles *Beil. J. Nanotechnol.* 1 182–90
- [69] Ouyang Z-W, Chen E-C and Wu T-M 2015 Thermal stability and magnetic properties of polyvinylidene fluoride/ magnetite nanocomposites *Materials* 8 4553–64

- [70] Dong Y-L, Zhang X-F, Cheng X-L, Xu Y-M, Gao S, Zhao H and Huo L-H 2014 Highly selective NO2 sensor at room temperature based on nanocomposites of hierarchical nanosphere-like α-Fe₂O₃ and reduced graphene oxide RSC Adv. 4 57493–500
- [71] Kudin K N, Ozbas B, Schniepp H C, Prud'homme R K, Aksay I A and Car R 2008 Raman spectra of graphite oxide and functionalized graphene sheets *Nano Lett.* 8 36–41
- [72] Strankowski M, Włodarczyk D, Piszczyk Ł and Strankowska J 2016 Polyurethane nanocomposites containing reduced graphene oxide, FTIR, Raman, and XRD Stud. J. Spectrosc. 2016 7520741
- [73] Shen M, Cai H, Wang X, Cao X, Li K, Wang S H, Guo R, Zheng L, Zhang G and Shi X 2012 Facile one-pot preparation, surface functionalization, and toxicity assay of APTS-coated iron oxide nanoparticles *Nanotechnology* 23 105601
- [74] Ossonon B D and Bélanger D 2017 Synthesis and characterization of sulfophenyl-functionalized reduced graphene oxide sheets RSC Adv. 7 27224–34
- [75] Li Y, Xie Q, Hu Q, Li C, Huang Z, Xiangjun Y and Guo H 2016 Surface modification of hollow magnetic Fe₃O₄@NH2-MIL-101(Fe) derived from metal-organic frameworks for enhanced selective removal of phosphates from aqueous solution Sci. Rep. 6 30651
- [76] Ng Y T, Kong W and Kong I 2018 Magnetite-functionalized graphene nanohybrids: preparation and characterization of electrical and magnetic property *Mater. Today Proc.* 5 3202–10
- [77] Xu J, Ju C, Sheng J, Wang F, Zhang Q, Sun G and Sun M 2013 Synthesis and characterization of magnetic nanoparticles and its application in lipase immobilization *Bull. Korean Chem. Soc.* 34 2408–12

- [78] Morteza Naghib S 2016 Novel magnetic nanocomposites comprising reduced graphene oxide/Fe₃O₄/gelatin utilized in ultrasensitive non- enzymatic biosensing *Int. J. Electrochem. Sci.* 11 10256–69
- [79] Bai L, Yuan R, Chai Y, Yuan Y, Wang Y and Xie S 2012 Direct electrochemistry and electrocatalysis of a glucose oxidase-functionalized bioconjugate as a trace label for ultrasensitive detection of thrombin *Chem. Commun.* 48 10972–4
- [80] Al-Sagur H, Komathi S, Karakaş H, Atilla D, Gürek A G, Basova T, Farmilo N and Hassan A K 2018 A glucose biosensor based on novel lutetium bis-phthalocyanine incorporated silica-polyaniline conducting nanobeads Biosens. Bioelectron. 102 637–45
- [81] Liang Y, Feng H, Shen D, Li N, Guo K, Zhou Y, Xu J, Chen W, Jia Y and Huang B 2017 Enhancement of anodic biofilm formation and current output in microbial fuel cells by composite modification of stainless steel electrodes J. Power Sources 342 98–104
- [82] Katuri K P, Kavanagh P, Rengaraj S and Leech D 2010 Geobacter sulfurreducens biofilms developed under different growth conditions on glassy carbon electrodes: insights using cyclic voltammetry Chem. Commun. 46 4758–60
- [83] Yuan Y, Zhao B, Zhou S, Zhong S and Zhuang L 2011 Electrocatalytic activity of anodic biofilm responses to pH changes in microbial fuel cells *Bioresource Technol*. 102 6887–91
- [84] Lower B H, Shi L, Yongsunthon R, Droubay T C, McCready D E and Lower S K 2007 Specific bonds between an iron oxide surface and outer membrane cytochromes MtrC and OmcA from Shewanella oneidensis MR-1 J. Bacteriol. 189 4944–52